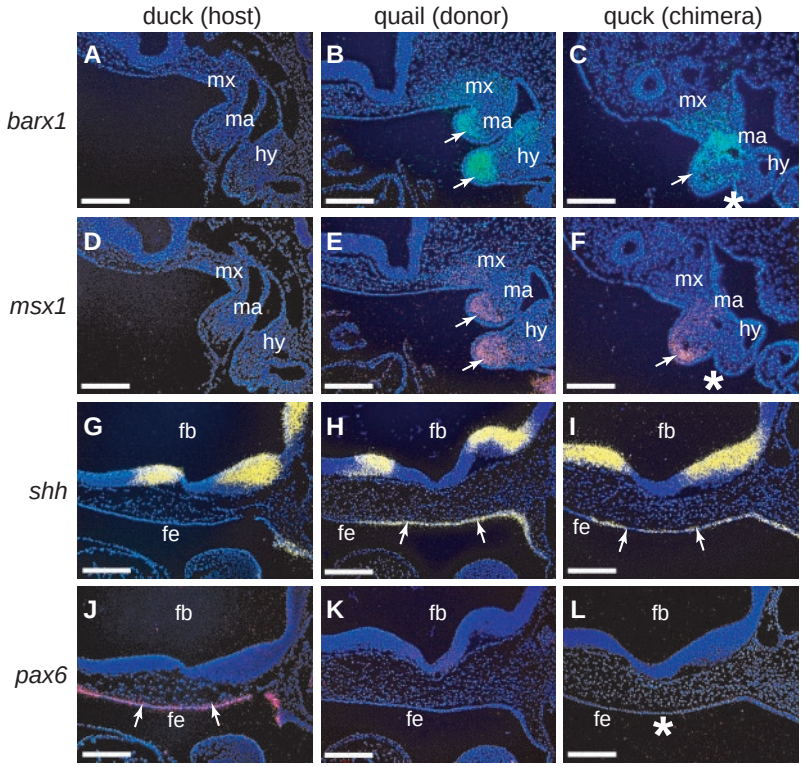

Fig. 4. Neural crest cell–autonomous molecular programs and regulation of gene expression in host facial ectoderm. (**A** to **F**) Twenty-four hours after surgery, control quails express *barx1* (green) and *msx1* (orange) in neural crest (arrows) of the maxillary (mx), mandibular (ma), and hyoid (hy) primordia, but control ducks do not yet express these genes. Quck chimeras at a stage equivalent to control ducks express *barx1* and *msx1*. Expression of these genes was not detected in quck hyoid cells (asterisks). (**G** to **L**) Forty-eight hours after surgery, control quails express *shh* (yellow) but not *pax6* (pink; arrows) in facial ectoderm (fe). Control ducks express *pax6* (arrows) but not *shh*. In quck chimeras stage-matched to control ducks, *shh* is detected (arrows) in duck host facial ectoderm but *pax6* (asterisk) is not. fb, forebrain neuroepithelium. Scale bar, 200 μm.

ral crest cells by surrounding tissues. In our experiments, the host environment may facilitate beak transformations by providing inductive signals that activate certain species-specific programs intrinsic to donor neural crest. Such a mechanism was anticipated by Hans Spemann's 19th-century work on inductive interactions of tissues. Spemann explains that after an interspecific transplant, the responding grafted tissue says to its inducer, "you tell me to make a mouth; all right, I'll do so, but I can't make your kind of mouth; I can make my own and I'll do that" (*22*). Thus, in terms of beak evolution, the neural crest appears to act as a conduit through which species-specific adaptations are implemented, and in this capacity neural crest cells may play an essential role by serving as responsive targets of natural selection.

References and Notes

1. C. Darwin, *On the Origin of Species* (Crowell-Collier, New York, 1859; 1962 ed.).
2. P. A. Trainor, P. P. Tam, *Development* **121**, 2569 (1995).
3. D. M. Noden, *Dev. Biol.* **67**, 296 (1978).
4. G. F. Couly, P. M. Coltey, N. M. Le Douarin, *Development* **117**, 409 (1993).
5. S. C. Ahlgren, M. Bronner-Fraser, *Curr. Biol.* **9**, 1304 (1999).
6. R. A. Schneider, D. Hu, J. L. Rubenstein, M. Maden, J. A. Helms, *Development* **128**, 2755 (2001).
7. J. A. Helms *et al.*, *Dev. Biol.* **187**, 25 (1997).
8. D. Hu, J. A. Helms, *Development* **126**, 4873 (1999).
9. T. Piotrowski, C. Nusslein-Volhard, *Dev. Biol.* **225**, 339 (2000).
10. G. Couly, S. Creuzet, S. Bennaceur, C. Vincent, N. M. Le Douarin, *Development* **129**, 1061 (2002).
11. See supporting data on *Science* Online.
12. V. Hamburger, H. L. Hamilton, *J. Morphol.* **88**, 49 (1951).
13. R. A. Schneider, *Dev. Biol.* **208**, 441 (1999).
14. A. M. Lucas, P. R. Stettenheim, *Avian Anatomy: Integument*, Agricultural Handbook 362, USDA Agricultural Research Service (U.S. Department of Agriculture, Washington, DC, 1972).
15. R. Coppinger, R. Schneider, in *The Domestic Dog*, J. Serpell, Ed. (Cambridge Univ. Press, Cambridge, 1995), pp. 21–47.
16. M. Mina, J. Gluhak, W. B. Upholt, E. J. Kollar, B. Rogers, *Dev. Dyn.* **202**, 195 (1995).
17. A. J. Barlow, J. P. Bogardi, R. Ladher, P. H. Francis-West, *Dev. Dyn.* **214**, 291 (1999).
18. Y. Shigetani, Y. Nobusada, S. Kuratani, *Dev. Biol.* **228**, 73 (2000).
19. G. Andres, *Genetics* **24**, 387 (1949).
20. G. Wagner, *Roux Archiv EntwMech. Organ.* **151**, 136 (1959).
21. G. S. Sohal, *Brain Res.* **113**, 35 (1976).
22. R. G. Harrison, *Am. Nat.* **67**, 306 (1933).
23. G. Köntges, A. Lumsden, *Development* **122**, 3229 (1996).
24. We thank D. Awai, M. Tong, J. Chou, and D. Hu for technical assistance and L. de la Fuente, B. Eames, and R. Marcucio for help with manuscript preparation. The anti-quail antibody (Q¢PN) was from the Developmental Studies Hybridoma Bank at the University of Iowa (National Institute of Child Health and Human Development grant NO1-HD-7-3263). Supported by National Institute of Dental and Craniofacial Research (NIDCR) grants T32 DE07236 and R03 DE014795-01 and a University of California San Francisco Research Evaluation and Allocation Committee award (R.A.S.) and by NIDCR grants K02 DE 00421 and R29 DE12462-03 (J.A.H.).

Supporting Online Material
www.sciencemag.org/cgi/content/full/299/5606/565/DC1
Materials and Methods
Figs. S1 and S2
References and Notes

28 August 2002; accepted 3 December 2002

Functional Mapping of the Primate Auditory System

Amy Poremba,[1]* Richard C. Saunders,[2] Alison M. Crane,[3] Michelle Cook,[4] Louis Sokoloff,[4] Mortimer Mishkin[2]

Cerebral auditory areas were delineated in the awake, passively listening, rhesus monkey by comparing the rates of glucose utilization in an intact hemisphere and in an acoustically isolated contralateral hemisphere of the same animal. The auditory system defined in this way occupied large portions of cerebral tissue, an extent probably second only to that of the visual system. Cortically, the activated areas included the entire superior temporal gyrus and large portions of the parietal, prefrontal, and limbic lobes. Several auditory areas overlapped with previously identified visual areas, suggesting that the auditory system, like the visual system, contains separate pathways for processing stimulus quality, location, and motion.

The full extent of the monkey's auditory system remains unknown. The principal cortical areas that have been identified by neuronal recording occupy approximately the caudal two-thirds of the superior temporal gyrus (STG) (*1–3*), although small sectors have also been found in

other cortical and subcortical areas, including, for example, the inferior parietal (*4*, *5*) and the lateral prefrontal cortices (*6*–*8*), and the superior colliculus (*9*, *10*). Yet this cannot be the full extent of the auditory system, inasmuch as the caudal STG sends dense projections to the rostral STG as well as to numerous other cortical regions outside the sectors identified thus far (*1*, *11*–*13*).

In an earlier study (*14*), we mapped the monkey's entire visual system by comparing glucose utilization in an intact ("seeing") hemisphere and a visually deafferented ("blind") hemisphere of an awake animal passively viewing visual stimuli (*15*, *16*). Here, we used the same strategy in an attempt to map the entire auditory system of the monkey.

Three chair-trained, adult rhesus monkeys (*Macaca mulatta*) weighing 4.0 to 4.8 kg were prepared with unilateral ablations of the inferior colliculus and transection of the forebrain and tectal commissures to yield an intact ("hearing") and an acoustically isolated ("deaf") hemisphere in each animal. Five to 10 weeks later, the 2-[^{14}C]deoxyglucose (2-DG) method (*17*, *18*) was applied while the animals listened passively to a variety of acoustic stimuli (*16*) (fig. S1). The 2-DG autoradiographs generated by this method revealed hemispheric asymmetries in local cerebral glucose utilization (LCGU), thereby indicating which areas had participated in auditory processing during the experiment (Fig. 1) (*16*, *19*, *20*).

Overall, the results demonstrated that cortical auditory tissue occupies the entire extent of the STG from the caudal tip of the lateral sulcus to the rostral tip of the temporal pole, and from the fundus of the lateral sulcus to the fundus of the superior temporal sulcus, as well as parts of the limbic cortex and large portions of both the inferior parietal lobule and the prefrontal cortex (Table 1 and Fig. 2). Subcortical structures shown to be involved in auditory processing include not only the tectum and medial geniculate body but also parts of the amygdala and neostriatum.

Among the largest hemispheric asymmetries observed were those in the areas of the STG comprising the primary (core) and the secondary (belt and parabelt) auditory cortices (*1*) (Table 1). However, as indicated, metabolic asymmetries extended throughout the entire length of the STG (–4 to +20 in Fig. 2), including its rostral third (rSTG).

[1]Department of Psychology and Neuroscience Program, University of Iowa, Iowa City, IA 52242, USA. [2]Laboratory of Neuropsychology, National Institute of Mental Health, Bethesda, MD 20892, USA. [3]Center for Perceptual Systems, University of Texas, Austin, TX 78712, USA. [4]Laboratory of Cerebral Metabolism, National Institute of Mental Health, Bethesda, MD 20892, USA.

*To whom correspondence should be addressed. E-mail: amy-poremba@uiowa.edu

The rSTG contained a columnar pattern of activity (Fig. 3, A and B). This pattern, which was observed in all three animals throughout the lateral surface and dorsal bank of the rSTG in the intact hemisphere, was not seen elsewhere in this hemisphere (*21*, *22*), nor was it identifiable in the rSTG of the deafferented hemisphere. In two intact control animals (*23*), the columns in the rSTG were apparent in both hemispheres but were wider than in the intact hemisphere of the experimental monkeys and were separated by correspondingly narrower, relatively inactive columns (Fig. 3, C and D). The findings suggest that, in intact monkeys, the pattern

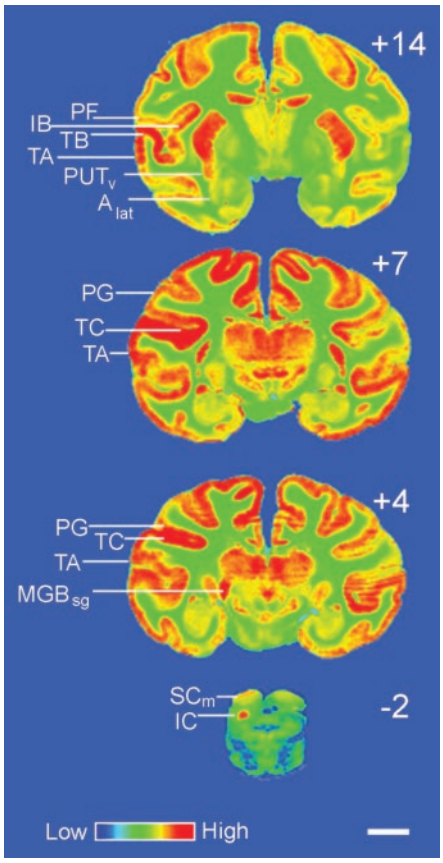

Fig. 1. 2-DG autoradiographs from a monkey prepared with a right inferior colliculus ablation (section –2) combined with forebrain and tectal commissurotomies, showing relative rates of glucose utilization in pseudocolor (see color bar). The left hemisphere is on the left. Numerals refer to the coronal levels of the sections in millimeters anterior (+) or posterior (–) to the interaural plane. Comparisons between the left, intact, hemisphere and the right, deafferented, hemisphere reveal the asymmetries indexing auditory regions, many of which are labeled. Scale bar, 5 mm. Cortical abbreviations are the cytoarchitectonic designations of Bonin and Bailey (*24*). Subcortical abbreviations are as follows: A_{lat}, lateral nucleus of the amygdala; IC, inferior colliculus; MGB_{sg}, medial geniculate body, including the supragenicule nucleus; PUT_v, ventral portion of the putamen; SC_m, midportion of the superior colliculus.

Table 1. Cortical and subcortical auditory regions. Values are means and standard errors of LCGU in micromoles per 100 g of tissue per minute in the three animals. For all structures listed, paired *t* tests indicated significantly greater LCGU in the intact hemisphere than in the deafferented hemisphere ($P < 0.05$). Percent difference in the final column was calculated as (intact – deafferented)/intact × 100. Cortical divisions in bold are those of Bonin and Bailey (*24*). Subdivisions of the core, belt, and parabelt areas listed under TC, TB, and TAc are based on those of Kaas and Hackett (*1*); the subdivision listed under TAr is that of Pandya (*12*); and subdivisions listed under FD, FDΔ, and FD/FF are those of Petrides and Pandya (*45*). The highest levels of glucose metabolism are found in two subdivisions of the core (A1 and R), which have also been shown to have the densest immunoreactivity for parvalbumin (*53*). For divisions with abbreviations: see Fig. 1; CD_t, tail of caudate nucleus; IA/IBd, dorsal one-third of insula; TAc, caudal two-thirds of TA; TAr, rostral one-third of TA; TAts, upper bank of superior temporal sulcus; TGd, dorsal one-half of TG. For locations of Bonin and Bailey divisions and of subcortical structures, see Figs. 1 and 2.

Divisions	Local glucose utilization (μmol/100 g/min)		
	Intact hemisphere	Deafferented hemisphere	% difference
Cortical			
TC, TB, TAc			
Al-core	77 ± 4	40 ± 3	46
R-core	73 ± 4	43 ± 5	42
RT-core	58 ± 3	33 ± 4	43
CM-belt	71 ± 1	47 ± 1	34
CL-belt	58 ± 2	43 ± 3	26
MM-belt	67 ± 2	45 ± 3	33
ML-belt	61 ± 1	46 ± 2	25
RM-belt	65 ± 4	48 ± 5	26
AL-belt	82 ± 6	46 ± 4	44
RTM-belt	58 ± 3	33 ± 4	43
RTL-belt	50 ± 4	36 ± 5	29
CPB-parabelt	67 ± 5	45 ± 4	31
RPB-parabelt	56 ± 5	46 ± 5	19
TAr			
TS2	54 ± 2	38 ± 1	30
TGd	44 ± 6	31 ± 4	30
TAts	53 ± 4	47 ± 2	12
TH	46 ± 2	41 ± 1	11
TF	47 ± 1	42 ± 3	11
PG	49 ± 3	42 ± 1	14
PF	47 ± 2	41 ± 1	13
LC	55 ± 3	49 ± 2	11
LA	52 ± 1	47 ± 3	10
IA/IBd	50 ± 2	44 ± 2	12
FD, FD_Δ			
Area 10	58 ± 4	52 ± 2	10
Area 46, 9/46	61 ± 2	54 ± 3	11
Area 45	62 ± 3	53 ± 1	15
Area 47/12	60 ± 2	52 ± 1	13
FD/FF			
Area 13	63 ± 5	53 ± 4	16
Subcortical			
MGB_{sg}	59 ± 2	41 ±2	31
SC_m	48 ± 3	42 ± 4	13
A_{lat}	43 ± 1	38 ± 3	12
CD_t	49 ± 1	44 ± 3	10
PUT_V	51 ± 2	45 ± 2	12

consists of adjacent thick and thin columns representing ipsilateral and contralateral auditory inputs, respectively, and of a third, thin, unactivated column.

Outside the STG, which includes cytoarchitectonic areas TC, TB, TA, and the dorsal TG (*24*), the only area in the temporal lobe that showed metabolic activation was the posterior parahippocampal region; here, the activated tissue was located in parts of area TF (+2 to +8, relative to the interaural plane, in Fig. 2) and TH (+2 in Fig. 2). Other activated limbic cortices included a small patch of area LC in the retrosplenial region (+2 in Fig. 2), and, widely separated from this, a long strip of area LA in the anterior cingulate gyrus just below the callosomarginal sulcus (+14 to +32 in Fig. 2).

Within the parietal lobe, the active area covered approximately the rostral two-thirds of the inferior parietal lobule, comprising portions of both areas PG and PF (–4 to +8 in Fig. 2). This activation extended into the dorsal part of the caudal insula, areas IA and IB (+8 to +2 in Fig. 2). Finally, the active frontal lobe tissue included a substantial portion of areas FD and FF in the orbitofrontal (+26 to +32 in Fig. 2) and inferior frontal cortex (+32 in Fig. 2) and, separated from these, a strip within areas FDΔ and FD along the upper bank and lip of the principal sulcus (+32 in Fig. 2).

The subcortical structures activated, beyond the major auditory relay nuclei, were the mid-portion of the superior colliculus (probably corresponding to the intermediate layers), the lateral nucleus of the amygdala, and parts of the ventral putamen and tail of the caudate nucleus (Fig. 1).

The boundaries of the metabolically active regions in the intact hemisphere were sometimes sharply delineated. This was the case, for example, for the rostral border in the inferior parietal lobule (+8 in Fig. 2), the medial border of the superior temporal gyrus at the level of the insula (+8 to +14 in Fig. 2), and the ventral border in the temporal pole (+20 in Fig. 2). In other locations, however, LCGU uptake tapered off only gradually across a cortical area. These latter locations were often regions in which the auditory maps overlapped with maps previously obtained in visual areas (*14*, *15*), as described below.

Comparison of the visual and auditory areas, in terms of where they do and do not overlap, suggests that the auditory system is organized along lines similar to those of the better-studied visual system. Previous work has identified three major multisynaptic corticocortical pathways or streams diverging from the striate cortex, each specialized for processing a different type of visual information: (i) An occipitotemporal or ventral stream dedicated to processing stimulus quality; (ii) an occipitoparietal or dorsal stream, concerned mainly with processing stimulus location; and (iii) a third stream coursing through the upper bank of the superior temporal sulcus, contributing (among other things) to processing stimulus motion (*25*, *26*). The present results suggest that an auditory region resembling and paralleling the unimodal, ventral visual pathway extends through the entire length of the supratemporal plane together with the exposed surface of the superior temporal gyrus (–4 to +20 in Fig. 2); like the ventral visual pathway, this auditory region appears to be modality-specific, suggesting that it is dedicated to analyzing acoustic stimulus quality for purposes of stimulus identification and recognition, just as the ventral visual pathway does for visual stimulus quality (*27*, *28*). In contrast, other large auditory sectors overlap extensively with visual areas. One such sector occupies the caudal half of the inferior parietal lobule

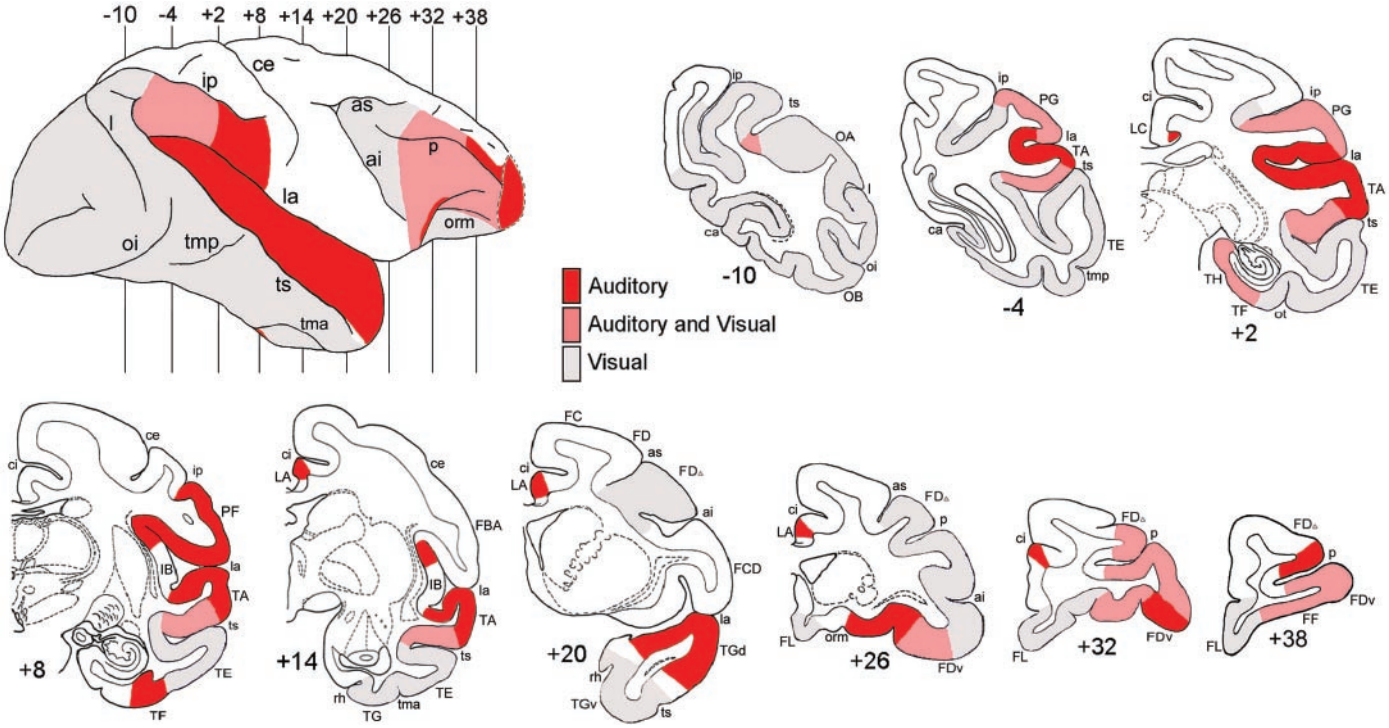

Fig. 2. Schematic summary of cortical areas related to the processing of auditory, auditory plus visual, and visual stimuli (red, pink, and gray areas, respectively), based on a comparison of the present results with those obtained in the earlier 2-DG visual experiment (*14*). Standard coronal sections through the right hemisphere are at levels indicated by the vertical lines on the lateral surface view (upper left). Numerals refer to number of millimeters anterior (+) or posterior (–) to the interaural plane. The frontal pole (FDE), surrounded by a dashed line, was not assessed for LCGU uptake in the 2-DG visual experiment. Boundaries were determined by visual inspection followed by quantitative examination of the autoradiographs for the individual cases, and the boundary positions were averaged across the cases within each study. Cortical abbreviations are the cytoarchitectonic designations of Bonin and Bailey (*24*). Sulcal abbreviations are as follows: ai, inferior limb of arcuate; as, superior limb of arcuate; ca, calcarine; ce, central; ci, cingulate; ip, intraparietal; l, lunate; la, lateral; oi, inferior occipital; orm, medial orbital; ot, occipitotemporal; p, principal; rh, rhinal; tma, anterior middle temporal; tmp, posterior middle temporal; and ts, superior temporal.

(–4 to +8 in Fig. 2), where it is coextensive with a substantial portion of the dorsal visual stream, whereas another extends through nearly the entire length of the upper bank of the superior temporal sulcus (–4 to +14 in Fig. 2) and is therefore coextensive with a major portion of the third visual stream. Multimodal processing in portions of these two sectors has been demonstrated physiologically (*2*, *5*). For example, a majority of a sample of neurons in the lower bank of the intraparietal sulcus (area LIP) (+2 in Fig. 2) have been found not only to be bimodal but also to show the same spatial tuning in their responses to the locations of auditory and visual stimuli (*5*). The present data are consistent with the notion that the two auditory sectors share the functions of the two visual pathways, which, therefore, are probably better viewed as contributing to an analysis of the location and motion, respectively, of both acoustic and visual stimuli.

Sharing of functions also applies to subcortical areas of auditory/visual overlap. Thus, the overlap in the middle layers of the superior colliculus is known to serve the elicitation of orienting to both visual and auditory stimuli (*9*, *10*), and, in the lateral amygdaloid nucleus, to mediate evocation of fear by particular stimuli in the two modalities (*29*, *30*). By implication, the overlap in the ventrocaudal neostriatum indicates that auditory input may mediate stimulus-response learning or habit formation in this modality, just as the visual input does in that modality (*31*).

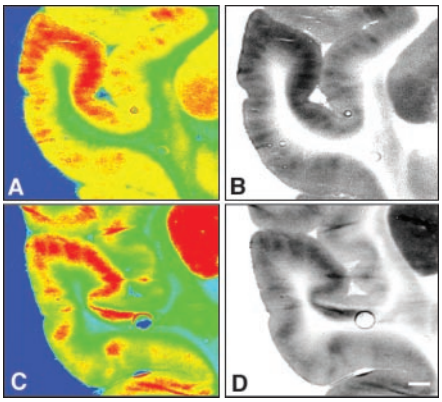

Fig. 3. 2-DG autoradiographs showing examples of acoustically activated columns within the rostral third of the left STG (TAr/TGd) from (**A** and **B**) the intact hemisphere of an experimental monkey, and (**C** and **D**) a control monkey. [(A) and (C) are pseudocolor renditions of autoradiographic images (B) and (D)]. In the coronal plane, the metabolically active columns in the experimental monkeys were 300 to 600 μm wide, separated by inactive columns 400 to 600 μm wide. Within each active column, the 2-DG uptake usually extended from layers II to V, being densest in layer IV. Reconstruction of these columns across several coronal sections revealed a stripelike pattern in the horizontal plane, with the active stripes extending 200 to 700 μm in the anterior-posterior direction, separated by 100- to 500-μm gaps. In the control monkeys, the columns were apparent in both hemispheres but were wider (500 to 800 μm) than in the intact hemisphere of the experimental monkeys and were separated by correspondingly narrower (200- to 400-μm) inactive columns. Scale bar in (D), 1 mm.

As in the case of the visual cortical pathways, the current data (+26 to +38 in Fig. 2) support the notion *(10)* that auditory cortical pathways continue into the prefrontal lobe, where only small sectors appear to be modality-specific. Auditory/visual overlap is also present at much earlier stages of cortical sensory processing, suggesting that cross-modal analysis and integration are likely to be serial/hierarchical processes just as it is in the case of unimodal analysis and integration. In some of the areas of sensory overlap, neuronal responses are enhanced by bimodal stimulation (*32*). Behaviorally, bimodal combinations of sensory input can markedly strengthen the detection and discrimination of stimuli and increase performance speed and accuracy (*33*, *34*).

Neuroimaging studies in humans (*35–41*) have revealed a substrate for auditory functions that is proportionately far more extensive than had been revealed heretofore in nonhuman primates (*42–45*). Some of these studies have implicated a dorsal pathway in the processing of sound sources (*37–40*), and a ventral pathway in the processing of tonal differences (*38*), environmental sounds (*37*), and verbal stimuli (*35*, *36*, *41*, *46*). By providing both a comprehensive and a high-resolution map of the auditory territory in the monkey, including evidence consistent with the notion of functionally different auditory processing streams, the present results help close the gap between the human and monkey cerebral auditory systems, in terms of both their extent and their organization. Perhaps more important, by delineating the many auditory regions in the monkey located beyond the primary and secondary auditory areas, the results lay the groundwork for an investigation of the likely neural substrates of higher-order auditory functions.

References and Notes

1. J. H. Kaas, T. A. Hackett, *Proc. Natl. Acad. Sci. U.S.A.* **97**, 11793 (2000).
2. C. Bruce, R. Desimone, C. G. Gross, *J. Neurophysiol.* **46**, 369 (1981).
3. B. Tian, D. Reser, A. Durhan, A. Kustov, J. P. Rauschecker, *Science* **292**, 290 (2001).
4. L. Leinonen, J. Hyvarinen, A. R. Sovijarvi, *Exp. Brain Res.* **39**, 203 (1980).
5. P. Mazzoni, R. M. Bracewell, S. Barash, R. A. Andersen, *J. Neurophysiol.* **75**, 1233 (1996).
6. L. M. Romanski, P. S. Goldman-Rakic, *Nature Neurosci.* **5**, 15 (2002).
7. J. D. Newman, D. F. Lindsey, *Exp. Brain Res.* **25**, 169 (1976).
8. J. M. Fuster, *The Prefrontal Cortex* (Raven, New York, ed. 2, 1989).
9. M. T. Wallace, M. A. Meredith, B. E. Stein, *Prog. Brain Res.* **112**, 301 (1993).
10. A. H. Bell, B. D. Corneil, M. A. Meredith, D. P. Munoz, *Can. J. Exp. Psychol.* **55**, 123 (2001).
11. L. M. Romanski *et al.*, *Nature Neurosci.* **2**, 1131 (1999).
12. D. N. Pandya, *Rev. Neurol. Paris* **151**, 486 (1995).
13. E. G. Jones, T. P. S. Powell, *Brain* **93**, 793 (1970).
14. K. A. Macko *et al.*, *Science* **218**, 394 (1982).
15. K. A. Macko, M. Mishkin, in *Brain Imaging and Brain Function*, L. Sokoloff, Ed. (Raven, New York, 1985).
16. Materials and methods are available as supporting material on *Science* Online.
17. L. Sokoloff *et al.*, *J. Neurochem.* **28**, 897 (1977).
18. C. Kennedy, O. Sakaruda, M. Shinohara, L. Sokoloff, *Ann. Neurol.* **4**, 293 (1978).
19. Adding an auditory behavioral requirement might reveal areas of activation beyond those reported here. However, when a behavioral requirement was introduced in a visual metabolic mapping study (*47*), no areas of activation were identified in addition to those found in response to passive viewing (*14*).
20. LCGU measurements were made of regions of interest throughout the cerebral hemispheres. The areas listed in Table 1 were the only ones that exhibited statistically significant hemispheric asymmetries.
21. An electrophysiological recording study (*48*) identified columns in the primary auditory cortex resulting from binaural summation and suppression.
22. Postmortem neuronal tract tracing of the interhemispheric projections of the human auditory cortex (Brodmann area 22) has shown regularly spaced clusters of neurons organized into columns (*49*).
23. Two control monkeys that had not been operated on were studied by the same methods as those used with the three experimental animals (*18*).
24. G. V. Bonin, P. Bailey, *The Neocortex of Macaca mulatta* (Univ. of Illinois Press, Urbana, IL, 1947).
25. L. G. Ungerleider, M. Mishkin, in *Analysis of Visual Behavior*, D. J. Ingle, M. A. Goodale, R. J. W. Mansfield, Eds. (MIT Press, Cambridge, MA, 1982), pp. 549–586.
26. D. Boussaoud, L. G. Ungerleider, R. Desimone, *J. Comp. Neurol.* **296**, 462 (1990).
27. Although this is likely to be true of much of the supratemporal plane and STG surface, other areas denoted here as auditory-only could overlap with somatosensory areas (*24*), as has previously been shown to occur in the secondary somatosensory cortex (*50–52*).
28. Evidence favoring the same division of function in the monkey is reviewed in (*11*, *46*).
29. H. Burton, G. Mitchell, D. Brent, *J. Comp. Neurol.* **210**, 109 (1982).
30. S. Campeau, M. Davis, *J. Neurosci.* **15**, 2312 (1995).
31. J. Fernandez-Ruiz, J. Wang, T. G. Aigner, M. Mishkin, *Proc. Natl. Acad. Sci. U.S.A.* **98**, 4196 (2001).
32. B. E. Stein, *Exp. Brain Res.* **123**, 124 (1998).
33. W. A. Teder-Saljarvi, J. J. McDonald, F. Di Russo, S. A. Hillyard, *Cognit. Brain Res.* **14**, 106 (2002).
34. G. A. Calvert, R. Campbell, M. J. Brammer, *Curr. Biol.* **10**, 649 (2000).
35. A. J. Saykin *et al.*, *Brain* **122**, 1963 (1999).
36. S. K. Scott, C. C. Blank, S. Rosen, R. J. Wise, *Brain* **123**, 2400 (2000).
37. P. P. Maeder *et al.*, *Neuroimage* **14**, 802 (2001).
38. C. Alain, S. R. Arnott, S. Hevenor, S. Grahan, C. L. Grady, *Proc. Natl. Acad. Sci. U.S.A.* **98**, 12301 (2001).
39. K. O. Bushara *et al.*, *Nature Neurosci.* **2**, 759 (1999).
40. T. D. Griffiths, G. G. Green, A. Rees, G. Rees, *Hum. Brain Mapp.* **9**, 72 (2000).
41. R. J. S. Wise *et al.*, *Brain* **124**, 83 (2001).
42. J. P. Rauschecker, B. Tian, M. Hauser, *Science* **268**, 111 (1995).
43. J. P. Rauschecker, *Audiol. Neurootol.* **3**, 86 (1998).
44. _____, *Curr. Opin. Neurobiol.* **8**, 516 (1998).
45. M. Petrides, D. N. Pandya, *Eur. J. Neurosci.* **11**, 1011 (1999).
46. J. P. Rauschecker, B. Tian, *Proc. Natl. Acad. Sci. U.S.A.* **97**, 11700 (2000).
47. H. E. Savaki, C. Kennedy, L. Sokoloff, M. Mishkin, *J. Neurosci.* **13**, 2772 (1993).

48. T. J. Imig, H. O. Adrian, *Brain Res.* **138**, 241 (1977).
49. R. A. Galuske, W. Schlote, H. Bratzke, W. Singer, *Science* **289**, 1946 (2000).
50. S. L. Juliano, P. J. Hand, B. L. Whitsel, *J. Neurophysiol.* **46**, 1260 (1981).
51. C. N. Woolsey, E. M. Walz, in *Cortical Sensory Organization, Multiple Auditory Areas*, C.N. Woolsey, Ed. (Humana, Totawa, NJ, 1982) vol. 3, pp. 231–256.
52. J. Kaas, C. E. Collins, *Curr. Opin. Neurobiol.* **11**, 498 (2001).
53. H. Kosaki, T. Hashikawa, J. He, E. G. Jones, *J. Comp. Neurol.* **386**, 304 (1997).
54. We thank S. Ghaznavi and H. J. Alitto for their assistance with the animals, and L. Ungerleider [National Institute of Mental Health (NIMH) and NIH] and J. Rauschecker (Georgetown University) for their critical reading of the manuscript and helpful suggestions. Supported by NIMH-IRP, NIH, and the U.S. Department of Health and Human Services.

Supporting Online Material
www.sciencemag.org/cgi/content/full/299/5606/568/DC1
Materials and Methods
Fig. S1

30 September 2002; accepted 4 December 2002

Extended Longevity in Mice Lacking the Insulin Receptor in Adipose Tissue

Matthias Blüher,[1] Barbara B. Kahn,[2] C. Ronald Kahn[1]*

Caloric restriction has been shown to increase longevity in organisms ranging from yeast to mammals. In some organisms, this has been associated with a decreased fat mass and alterations in insulin/insulin-like growth factor 1 (IGF-1) pathways. To further explore these associations with enhanced longevity, we studied mice with a fat-specific insulin receptor knockout (FIRKO). These animals have reduced fat mass and are protected against age-related obesity and its subsequent metabolic abnormalities, although their food intake is normal. Both male and female FIRKO mice were found to have an increase in mean life-span of ~134 days (18%), with parallel increases in median and maximum life-spans. Thus, a reduction of fat mass without caloric restriction can be associated with increased longevity in mice, possibly through effects on insulin signaling.

Longevity is dependent on many factors including genetics (*1*, *2*), hormonal and growth factor signaling (*3*, *4*), body weight (*5*), body fat content, and environmental factors (*4*, *6*). Food restriction is the most potent environmental variable and has been shown to increase longevity in diverse organisms (*6*). The effect of restricted feeding on life-span has been studied in rodents for more than 60 years (*7*–*10*), and although some studies have suggested that reduced food intake is more important than adiposity (*8*, *9*), it is difficult to separate the beneficial effect of caloric restriction from that of leanness and the various biochemical correlates of leanness.

To investigate this question, we evaluated the life-span of the fat-specific insulin receptor knockout (FIRKO) mouse. These animals were derived by crossing insulin receptor IR (lox/+) mice, in which exon 4 of the insulin receptor is flanked by loxP sites (*11*), with IR (lox/+) mice that also express the Cre recombinase under the control of the aP2 promoter/enhancer (*12*). This breeding strategy also generated three littermate control groups: wild-type (WT), IR (lox/lox), and aP2-Cre mice, which were indistinguishable with regard to physiologic and metabolic parameters and have the same mixed genetic background as the FIRKO mice. For the aging experiments, 250 animals were housed under the same conditions in a virus-free facility on a 12-hour light/dark cycle and were given a standard rodent feed and water ad libitum.

Growth curves were normal in male and female FIRKO mice from birth to 8 weeks of age. Starting at 3 months of age, FIRKO mice maintained 15 to 25% lower body weights and a 50 to 70% reduction in fat mass throughout life (Fig. 1A). The reduction in adiposity was estimated by perigonadal fat pad weight but was apparent in all fat depots and was also reflected by a reduction of ~25% in total-body triglyceride content (*13*). FIRKO mice are healthy, lack any of the metabolic abnormalities associated with lipodystrophy, and are protected against age-related deterioration in glucose tolerance, which is observed in all control strains (*13*). FIRKO mice maintained low body fat, despite normal food intake (Fig. 1B). Indeed, because FIRKO mice were leaner, the food intake of FIRKO mice expressed per gram of body weight actually exceeded that of controls by an average of 55% (Fig. 1C).

The median life-span of most laboratory

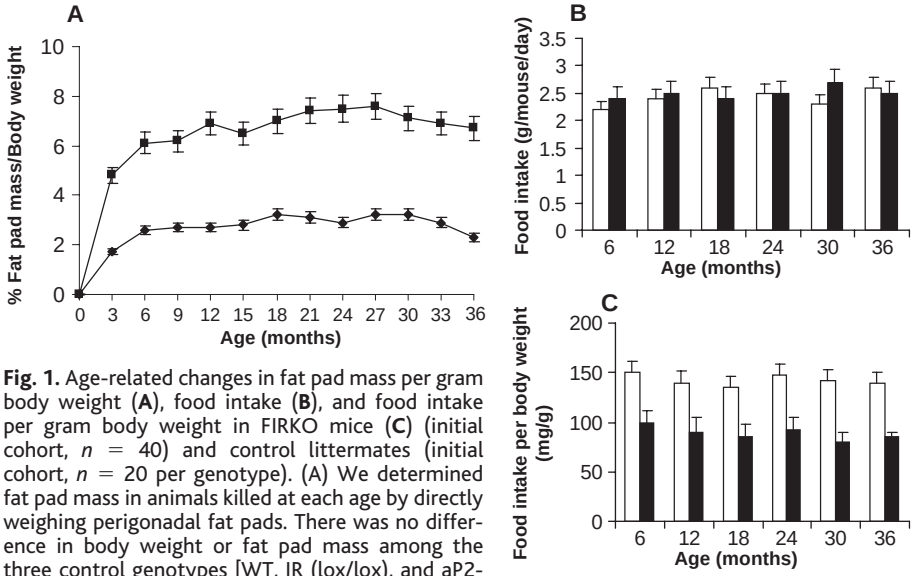

Fig. 1. Age-related changes in fat pad mass per gram body weight (**A**), food intake (**B**), and food intake per gram body weight in FIRKO mice (**C**) (initial cohort, $n = 40$) and control littermates (initial cohort, $n = 20$ per genotype). (A) We determined fat pad mass in animals killed at each age by directly weighing perigonadal fat pads. There was no difference in body weight or fat pad mass among the three control genotypes [WT, IR (lox/lox), and aP2-Cre]. After the mice reached the age of 3 months, the differences in fat pad mass per gram of body weight were significant for all data points between FIRKO mice (diamonds) and all three controls (squares) ($P < 0.05$). (B) In mice caged singly, we determined food intake (gram per mouse per day) daily over 5 days by using at least five FIRKO (white bars) and four control mice (black bars) per genotype ($n = 12$). Data of the control genotypes [WT, IR (lox/lox), and aP2-Cre] are plotted together in the black bars, because there were no differences in daily food intake among them. (**C**) Food intake per gram body weight—calculated from the food intake and body weight data—was significantly increased in FIRKO mice (white bars) as compared with controls (black bars) ($P < 0.05$).

[1]Joslin Diabetes Center and Department of Medicine, Harvard Medical School, One Joslin Place, Boston, MA, 02215 USA. [2]Department of Medicine, Beth Israel Deaconess Medical Center and Harvard Medical School, Boston, MA, 02215 USA.

*To whom correspondence should be addressed. E-mail: c.ronald.kahn@joslin.harvard.edu